JVST A
Journal of Vacuum Science & Technology A

Impact of encapsulation method on the adsorbate induced electrical instability of monolayer graphene

Cite as: J. Vac. Sci. Technol. A **37**, 051502 (2019); https://doi.org/10.1116/1.5099141
Submitted: 07 April 2019 • Accepted: 10 July 2019 • Published Online: 25 July 2019

Sırrı Batuhan Kalkan, Alper Yanilmaz and Cem Çelebi

View Online

Export Citation

CrossMark

ARTICLES YOU MAY BE INTERESTED IN

The effect of adsorbates on the electrical stability of graphene studied by transient photocurrent spectroscopy
Applied Physics Letters **112**, 013103 (2018); https://doi.org/10.1063/1.5011454

Tailoring commensurability of hBN/graphene heterostructures using substrate morphology and epitaxial growth conditions
Journal of Vacuum Science & Technology A **37**, 051503 (2019); https://doi.org/10.1116/1.5110524

Low energy electron interactions with 1-decanethiol self-assembled monolayers on Au(111)
Journal of Vacuum Science & Technology A **37**, 051401 (2019); https://doi.org/10.1116/1.5098946

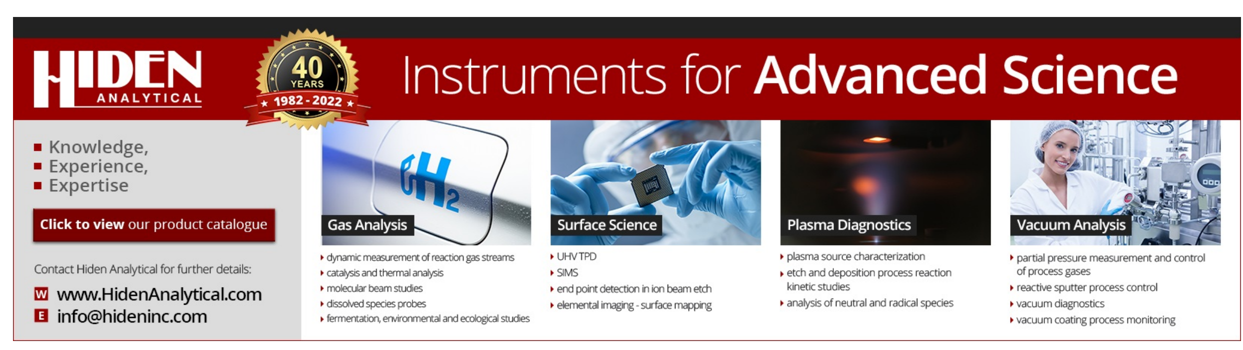

© 2019 Author(s).

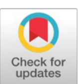

Impact of encapsulation method on the adsorbate induced electrical instability of monolayer graphene

Sırrı Batuhan Kalkan, Alper Yanilmaz, and Cem Çelebi[a)]
Quantum Device Laboratory, Department of Physics, İzmir Institute of Technology, 35430 İzmir, Turkey

(Received 7 April 2019; accepted 10 July 2019; published 25 July 2019)

Monolayer graphene transferred onto a set of silicon carbide (SiC) substrates was encapsulated with a thin SiO_2 film in order to prevent its interaction with atmospheric adsorbates. The encapsulation of graphene samples was realized by using two different thin film growth methods such as thermal evaporation (TE) and state-of-the-art pulsed electron deposition (PED). The encapsulation efficiency of these two techniques on the structural and electrical characteristics of graphene was compared with each other. Scanning electron microscopy (SEM) analysis showed that unlike the SiO_2 thin film grown with PED, structural defects like cracks were readily formed on TE grown films due to the lack of surface wettability. The electronic transport measurements revealed that the electrical resistivity of graphene has been increased by two orders of magnitude, and the carrier mobility has been subsequently decreased upon the encapsulation process with the PED method. However, in-vacuum transient photocurrent spectroscopy (TPS) measurements conducted for short periods and a few cycles showed that the graphene layer encapsulated with the PED grown SiO_2 film is electrically far more stable than the one encapsulated with TE grown SiO_2 film. The results of TPS measurements were related to the SEM images to unravel the mechanism behind the improved electrical stability of graphene samples encapsulated with the PED grown SiO_2 film. *Published by the AVS.*
https://doi.org/10.1116/1.5099141

I. INTRODUCTION

Graphene has been considered a wonder material for its unique electronic and mechanical features that lead the way for the adaptation of graphene and graphenelike other two-dimensional (2D) materials in novel electronic and optoelectronic device applications.[1–4] Owing to its large surface area-to-volume ratio, the susceptibility of graphene to various gases has promoted the integration of graphene in gas sensing technology.[5] However, these ideas have been inhibited by physical limitations such as the long-term electrical stability of graphene under ambient conditions. The interaction of graphene with atmospheric adsorbates like O_2 and H_2O directly affects the temperature sensing, Schottky diode, and field effect transistor properties of graphene-based devices.[6,7] The electrical stability of such devices can be guaranteed only by the suppression of these interactions. A number of different materials[8–13] like parylene, polymethyl methacrylate, and hexagonal boron nitride have been employed as encapsulating materials in order to improve the electrical stability of graphene by isolating it from ambient gas molecules. Besides, different dielectric materials (mostly Al_2O_3 and HfO_2) with high-k dielectric constants[14–20] have also been used to passivate the graphene layer to achieve reliable device performance.[21] Although the encapsulation and/or passivation of graphene with above mentioned materials seems to be a reasonably simple task, it turns out to be a great challenge in practice.

One of the major issues arises from the characteristics of the surface that is intended to be passivated. The wettability of the surface can significantly affect the quality and durability of the passivation layer on it. The hydrophobic surface is known to be very problematic, as the encapsulation can fail due to low surface tension.[22] Pristine graphene presents a typical example as a hydrophobic surface because of its inert nature.[23,24] It has been demonstrated that water can easily be adsorbed onto the edges of graphene sheets;[25,26] thus, the presence of polar oxygen groups like OH^- converts graphene into a hydrophilic material.[27] In addition, the dangling bonds and defects like carbon vacancies, sp^3 sites, C–H or OH^- bonds can be created on the graphene layer as a result of oxygen plasma treatment, and thus the surface energy can be boosted.[28–30] The increment in surface energy converts hydrophobicity into hydrophilicity. Therefore, the adhesivity and/or wettability of graphene can be improved and controlled by optimizing the plasma power and exposure time of oxygen plasma treatment.[27] It should be noted that the exposure time and plasma power must be carefully tuned in order to substantially minimize any possible damage on the graphene layer.

Silicon dioxide (SiO_2) is a prevalent and relatively cheap dielectric material for surface coatings because of its excellent antireflective[31] and moisture resistant[32] capabilities. The coating of surfaces with an SiO_2 layer can be realized by common thin film deposition techniques including sputtering, thermal evaporation (TE), and pulsed electron deposition (PED). The deposition and coating efficiency of these methods for passivating graphene must be carefully examined in order to assess the effect of hydrophobicity on the encapsulation quality. This is crucially important for choosing the suitable passivation method and thus for improving the electrical stability of graphene-based devices.

[a)]Electronic mail: cemcelebi@iyte.edu.tr

 0734-2101/2019/37(5)/051502/6/$30.00

In this study, we present a detailed comparison of two encapsulation methods (TE and PED) for suppressing the interactions between atmospheric adsorbates and graphene. For the experiments, CVD-grown graphene layers on Cu foil is transferred onto semi-insulating (SI) SiC substrates, and then 100 nm thick SiO_2 film was deposited on top of it as the encapsulation layer. The structural properties of bare (BG) and SiO_2 encapsulated graphene layers were analyzed by Raman spectroscopy, atomic force microscopy (AFM), and scanning electron microscopy (SEM) measurements. The electrical (resistivity and Hall measurements) and optoelectronic characterizations [transient photocurrent spectroscopy (TPS)] were carried out for evaluating the passivation efficiency on the electrical stability of graphene. We found that defects like cracks are formed on the TE SiO_2 film due to the hydrophobicity of graphene layer underneath. On the other hand, a smooth coating of SiO_2 is obtained with the PED technique owing to low energy plasma occurring during the deposition process, which changes the hydrophobicity of graphene without giving any structural damage. The TPS measurements are in good agreement with the results of SEM characterizations. Although an improvement in the measured photocurrent was achieved after TE encapsulation, rectified and sharp TPS transitions were observed for PED SiO_2 graphene samples. The experimentally obtained results showed that surface treatment with low energy O_2 plasma increases the surface tension of graphene and, therefore, improves the passivation capability of the deposited SiO_2 thin film.

II. EXPERIMENT

A. Growth, transfer, and encapsulation of graphene

Large area graphene samples were grown on unpolished copper (Cu) foil (25 μm thick, 99.8% purity, Alfa Aesar) by an atmospheric pressure chemical vapor deposition system. Prior to the graphene growth experiments, Cu foil was annealed for an hour at a temperature of 1000 °C under an H_2 (20 sccm) and Ar (1000 sccm) gas mixture with a temperature ramp rate of 30 °C min^{-1}. After the annealing process, CH_4 (10 sccm) gas was introduced into the furnace for 2 min. in order to obtain single layer graphene. Finally, the sample was left for a rapid cool down to room temperature under H_2 (20 sccm) and Ar (1000 sccm) gas flows.

The photoresist (PR) drop casting method is used for the graphene transfer procedure. Thick droplets of S1813 PR chemical were drop-casted on graphene and baked at 70 °C overnight to gently harden the PR itself. The baked sample was then immersed in an $FeCl_3$ solution to etch the Cu foil underneath the graphene/PR bilayer. The Cu-free graphene/PR stack was cleaned in deionized water to remove the $FeCl_3$ residue. After N_2 drying, the stack was transferred onto the SI-SiC substrate. Then, the substrates were baked at 110 °C to reflow the PR on graphene, which helps the PR to liquefy and release the graphene layer. The thermally softened PR on graphene was removed in acetone.

The SiO_2 encapsulation of the graphene layer transferred on SI-SiC was realized by using TE and PED techniques. The TE method is based on the direct sublimation of SiO_2 pellets placed in a tungsten boat via Joule heating, while PED is a gas assisted plasma deposition technique in which SiO_2 is ablated from a high purity commercial sputtering target (Kurt J. Lesker, 99.999%) using a high power pulsed electron beam. Prior to the encapsulation process, each of the samples was annealed at 120 °C in vacuum to remove the residues and possible adsorbates left from the transfer process done under atmospheric environment. The sublimation power used for SiO_2 evaporation was 240 W, which corresponds to a temperature of about 1600 °C in a pressure range of around 2×10^{-7} mbar. The growth parameters of PED were 9.5 kV discharge voltage and 5.5 mTorr O_2 gas pressure. 100 nm thick SiO_2 film was deposited on two sets of graphene layers with TE and PED techniques, separately.

B. Electronic and optoelectronic characterization

For resistivity and Hall effect measurements, 4-terminal contacts comprising Cr (~3 nm)/Au (~80 nm) contact pads are deposited thermally on the corners of square shaped samples in order to conduct 4-probe measurements through a van der Pauw geometric structure.[33,34] The electrical characterizations of samples were done by using a Keithley 6220 Precision Current Source and a Keithley 2000 Digital Multimeter. A permanent neodymium magnet providing a magnetic field of 0.33 T was used for Hall Effect measurements. Current–voltage (I–V) measurements were carried out by a Keithley 2400 SMU and a 6485 Picoammeter. In addition, 254 nm UV light with 3 mW output power is used as the light source for optoelectronic and TPS experiments. All the measurements were done under high vacuum conditions.

III. RESULTS AND DISCUSSION

A. Raman and AFM analysis of CVD-grown graphene

The number of graphene layers was determined by single point Raman spectroscopy measurements right after the growth. Figure 1(a) shows the Raman spectrum of CVDG including D (1369 cm^{-1}), G (1590 cm^{-1}), and 2D peaks (2718 cm^{-1}). The strong G peak and the weak D peak indicate good graphitic quality, and the large 2D to G peak intensity ratio ($I_{2D}/I_G > 2$) confirms the monolayer nature of CVDG.[35] The obtained Raman spectrum reveals that both intensity ratios and narrow full width at half maximum of the 2D peak verify the existence of transferred single layer CVDG.[36,37] The AFM topography image of CVDG on the SI-SiC substrate can be seen in Fig. 1(b). The CVDG layer contains wrinkles and residues originating both from the growth procedures and PR assisted transfer of CVDG from Cu foil onto the SiC substrate.[21]

B. SEM analysis of SiO_2 encapsulated graphene

SEM images of BG, TE-encapsulated (TEG), and PED-encapsulated graphene (PEDG) are shown in Figs. 2(a)–2(c), respectively. For a better inspection of the sample surface, magnified SEM images are displayed in Figs. 2(d)–2(f).

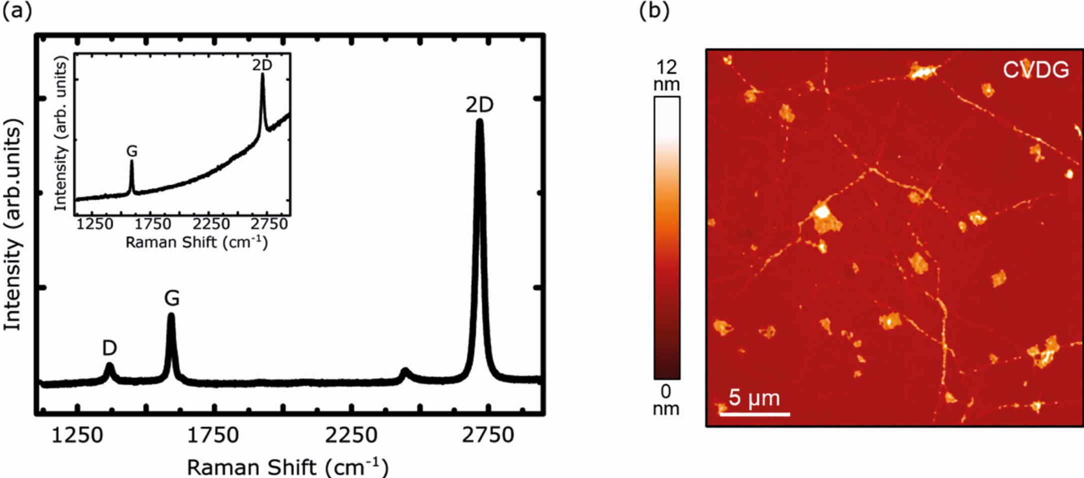

FIG. 1. (a) Raman spectrum of Cu background subtracted bare CVDG (the inset shows the Raman spectrum of the graphene layer on Cu foil). (b) AFM topography image of bare CVDG on the SI-SiC substrate.

As seen in Fig. 2(b), cracks are formed throughout the surface of the thermally evaporated SiO_2 film on the graphene layer. The reason is that the large thermal expansion coefficient difference between the SiO_2 thin film ($\alpha_{SiO_2} = 5 \times 10^{-6}\,K^{-1}$)[38] and graphene ($\alpha_{graphene} = -8 \times 10^{-6}\,K^{-1}$)[39] causes a substantially high mechanical strain and stress, which gives rise to the observed deformations on the SiO_2 layer. However, a smooth coating of the SiO_2 film on graphene is obtained using the PED technique. As the graphene layer was exposed to an *in situ* low energy O_2 plasma during SiO_2 deposition in a PED chamber, its surface energy is increased. The boosted surface energy gives rise to hydrophilicity in the graphene layer after PED encapsulation, which prevents the formation of cracks in contrast to the TE method. These results manifest that the surface wettability plays an important role in the structural and morphological quality of the SiO_2 thin film, and O_2 plasma treatment improves the adhesivity of the surface and minimizes the surface deformations on the encapsulation layer.[40]

As seen in Figs. 2(e) and 2(f), the sizes of SiO_2 nanoparticles are different due to two distinct coating methods. The average size and amount of SiO_2 nanoparticulation are bigger and larger in TE encapsulation when compared to the nanoparticles formed during PED [compare Figs. 2(e) and 2(f)]. Graphene related wrinkles can also be seen in the high magnification SEM image [Fig. 2(f)] of PED grown SiO_2 on graphene. These observed wrinkles are clear indicators for the full coverage of a graphene layer. Contrary to

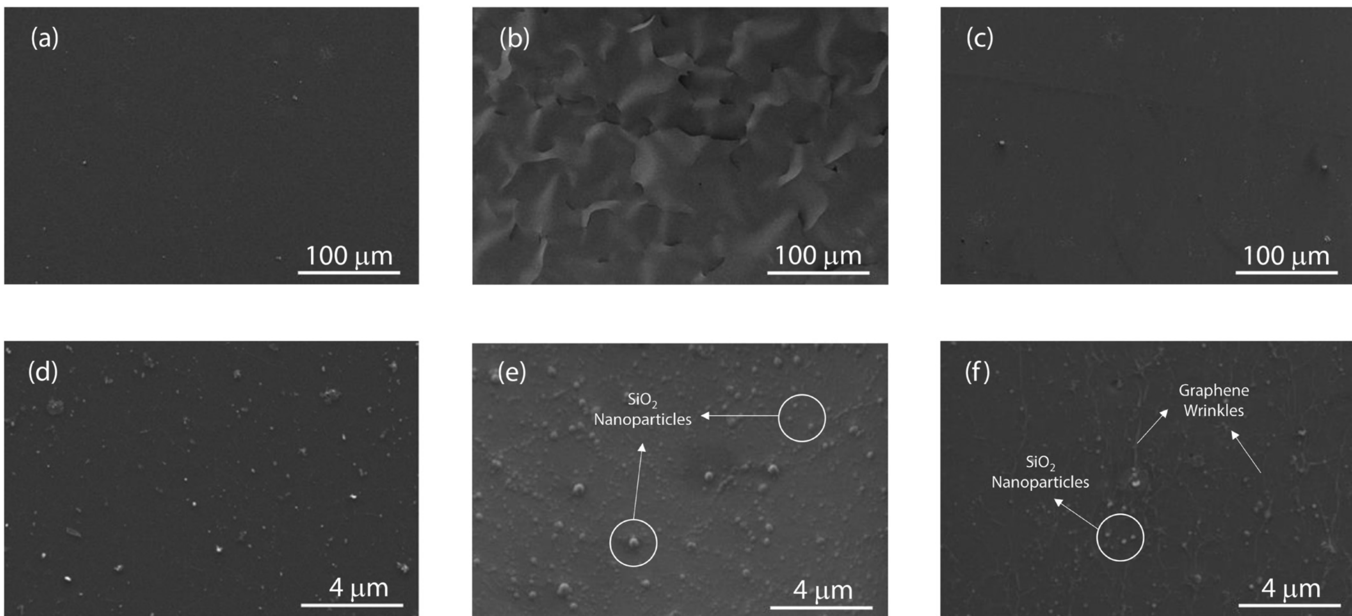

FIG. 2. SEM images of (a) BG, (b) TEG, and (c) PEDG showing the surface morphology of the SiO_2 encapsulation layer on graphene. Magnified SEM images of (d) BG, (e) TEG, and (f) PEDG samples.

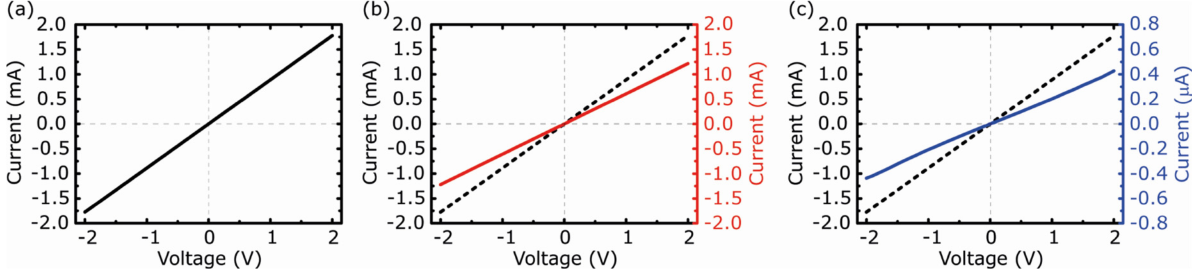

FIG. 3. I–V characteristics of (a) BG, (b) TEG, and (c) PEDG. The dashed line in (b) and (c) corresponds to the I–V measurement of BG as a reference.

PED SiO_2, graphene wrinkles are not resolved in the TE SiO_2 [Fig. 2(e)] encapsulation layer. Since graphene has a lack of wettability in the case of growth with the TE technique, the coating efficiency is reduced due to the absence of surface adhesion on the graphene layer.

C. Electronic transport characterizations

Prior to determining the charge carrier characteristics of the samples, we conducted two-terminal I–V measurements for both TEG and PEDG before and after the SiO_2 encapsulation process and the obtained results are compared in Figs. 3(a) and 3(b). The measurements were acquired at a bias voltage range between −2 V and 2 V. The initial resistance of BG was measured as 1.1 kΩ, and after the SiO_2 encapsulation with TE, its resistance was found to be increased to only 1.6 kΩ. However, in the case of SiO_2 encapsulation with PED, the resistance of the PEDG sample was determined to be as high as 4.7 MΩ. This observed increment in the resistance of PED SiO_2 samples was attributed to the passivation of dangling bonds responsible for the charge transport in the graphene layer.

One of the key measurement methods to investigate the electrical properties of materials is the combination of resistivity and Hall measurements. The sheet resistance and carrier density measurements were done on monolayer graphene before and after SiO_2 encapsulation of the samples by TE and PED techniques. For the electrical characterization steps, we produced a number of graphene samples. We found that the sheet resistance of all the grown graphene layers changes in between the values 1.2–3.5 kΩ/□. Therefore, the sheet carrier density and mobility values are also different depending on the graphene layer chosen. The sheet resistance, sheet carrier density, and the mobility values given in Table I for BG are typical. In other words, for the electronic transport measurements, two sets of graphene samples were selected randomly for comparing the effects of TE and PED encapsulation processes separately. We found that the sheet resistance of PED SiO_2 and TE SiO_2 encapsulated graphene is increased around two orders of magnitude and one order of magnitude, respectively. A dramatic decrement in the carrier density was also observed after the PED encapsulation process. The reduction in the carrier density is related to complete distraction of the atmospheric dopers from the graphene layer. In the TEG case, the SiO_2 encapsulation layer with defects cannot completely suppress the interaction of adsorbates with the graphene layer. The results of sheet resistance and sheet carrier density measurements showed that the mobility variations in the TEG are more acceptable compared to PEDG: A 25% decrement in the carrier mobility was measured after TE encapsulation (see Table I). It is known that the oxygen plasma treatment can degrade the carrier mobility because of both the increment in bonding strength and generation of dangling bonds.[41] Although the measured value for the carrier mobility of PEDG is much lower than that of BG, it can be concluded that the increment in sheet resistance and the decrement in carrier density are clear indicators for the complete passivation of the graphene layer with PED grown SiO_2 film. Compared to the encapsulation materials like Al_2O_3 and HfO_2 that were mentioned in the Introduction section,[16–18,42] the mobility of our PED SiO_2 encapsulated graphene samples is lower due to the low-k dielectric constant of the SiO_2 thin film.[43,44]

D. Transient photocurrent spectroscopy measurements

It is known that the adsorption/desorption of gas molecules like O_2 and H_2O is one of the main problems in terms of the electrical stability of low dimensional materials due to their high surface-to-volume ratio. There are several studies on the impact of these atmospheric adsorbates on graphene layers.[21,45] Owing to the PR assisted transfer process and the $FeCl_3$ etchant for copper etching, CVDG is unintentionally p-type doped.[46,47] The above-mentioned atmospheric adsorbates are known to dope CVDG with holes. In order to remove these adsorbates from the graphene layer, the samples were illuminated by a UV lamp for 10 ks under high vacuum ($P \sim 10^{-5}$ mbar) conditions.[48] Then, 30 s

TABLE I. Sheet resistance and carrier density characteristics of BG, TEG, and PEDG samples.

Method	Sheet resistance (kΩ/□)	Sheet carrier density (10^{12} cm^{-2})	Mobility (cm^2/V s)
BG	1.5	16.9	243.8
TEG	15.9	2.1	183.3
BG	3.1	13.9	134.2
PEDG	341.4	0.7	25.2

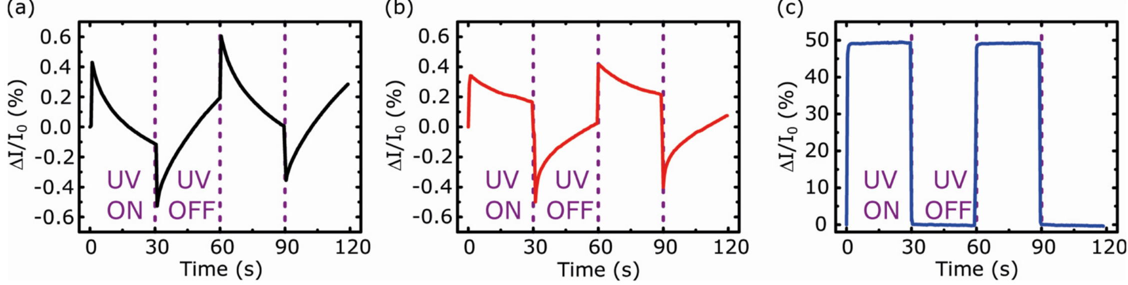

FIG. 4. Transient photocurrent spectroscopy measurements of (a) BG, (b) TEG, and (c) PEDG.

two-cycle photocurrent spectroscopy measurements were taken to investigate the contribution of the adsorbates to the electrical characteristics of graphene, as well as the contribution of the photogenerated excitons formed at the depletion layer of the underlying wide bandgap ($E_g = 3.2$ eV) SI-SiC substrate.

The TPS measurement of BG is shown in Fig. 4(a). When the UV light is turned on, a sudden peak related to the photogenerated exciton occurs, and then an exponential decay follows it over time due to the simultaneous desorption of hole doped atmospheric adsorbates. After the shutter is closed, the photogenerated charge carriers (electrons and holes) recombine, and thus a steep drop is observed within a fraction of 1 s. Since the partial pressure of H_2O and O_2 ($P \sim 10^{-8}$ mbar[49]) is much lower than the pressure level of our vacuum chamber ($P \sim 10^{-5}$ mbar), these adsorbates expelled from the graphene layer under vacuum start to stick back on the surface over time, which is reflected as a slow exponential growth in the measured current when the UV light is turned off as shown in Fig. 4. The contribution of adsorption/desorption of adsorbates in the measured current was found to be more dominant than the contribution of photogenerated charge carriers. This gives rise to an overall increment in the current alteration after two periods of on/off cycles. As seen in Fig. 4(b), the contribution of adsorption/desorption to the measured current becomes less pronounced after the SiO_2 encapsulation of graphene with the TE method.

For TE SiO_2 encapsulated graphene, the adsorbate effect seen as an exponential function of time still plays a crucial role. This is due to the cracks present on the SiO_2 film as shown in Fig. 2(b). The atmospheric adsorbates seem to interact with the graphene layer by penetrating from the cracks and cavities on the SiO_2 thin film. Unlike BG and TEG, the TPS measurement of the PEDG sample exhibits uniform and stable profiles, revealing that the sample had excellent photocurrent reversibility and a fast response speed [Fig. 4(c)]. The obtained result is in an agreement with the SEM measurement of PEDG. Since the interaction of adsorbates in air with graphene is blocked completely by the PED SiO_2 layer, the contributions of the photogenerated excitons to the electrical conductivity become dominant. Therefore, the photoswitching time is greatly enhanced and all transitions occurred within only a second. It can also be deducted from Fig. 4(c) that the amplitude of the photogeneration is increased about two orders of magnitude after PED encapsulation. This is due to the fact that the adsorbate layer absorbs most of the UV light due to its binding energy. Thus, the exciton generation rate in the depletion layer of underlying SI-SiC dramatically diminishes. However, successful passivation evacuates this adsorbate layer and thus the exciton generation rate can be increased substantially.

The schematic illustrations that describe the effect of the encapsulation methods on the adsorbate interactions are shown in Fig. 5. The cross-sectional sketches of the samples are combined with the top view SEM images that are given at the bottom of each illustration in Fig. 5. As illustrated in Fig. 5(a), the adsorbates readily stick on the graphene layer and thus increase their electrical conductivity. After TE encapsulation, SiO_2 flakes partially hinder the sticking of adsorbates on the graphene layer. Accordingly, the effective surface-to-volume ratio is decreased [see Fig. 5(b)] and the conductivity fluctuations are enhanced. However, the interactions between the graphene layer and atmospheric adsorbates could not be stabilized completely. A complete suppression is only achieved by PED encapsulation, thanks to its in situ low energy plasma treatment that increases the surface energy and overcomes the thermal expansion coefficient difference between graphene and SiO_2 [Fig. 5(c)].

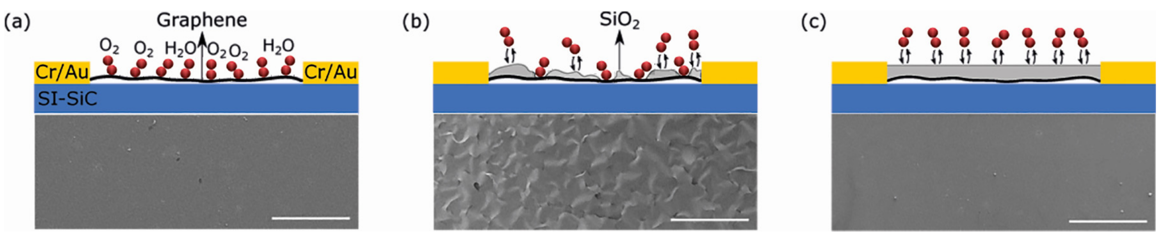

FIG. 5. Schematics of the mechanism for (a) BG, (b) TEG, and (c) PEDG. The scale bar of all the SEM images is 200 μm.

IV. SUMMARY AND CONCLUSIONS

The impact of atmospheric adsorbates on the electronic and optoelectronic characteristics of graphene is investigated by encapsulating the graphene layer with two different coating methods. The measurements show that the surface wettability plays a crucial role in the encapsulation efficiency of the deposited SiO_2 thin film. We observed that cracks are formed throughout the surface of the thermally evaporated SiO_2 film on graphene as a result of poor surface wetting. The cracks on thermal SiO_2 passivate graphene only partially and thus reduce the effective surface area-to-volume ratio of encapsulated graphene compared to that of bare graphene. On the contrary to TE, graphene is exposed to low energy plasma treatment during the PED process, which increases the surface energy and greatly suppresses the cracks on the deposited SiO_2 film. The encapsulation of graphene with PED grown SiO_2 was found to decrease the carrier mobility relative to the carrier mobility of TE SiO_2 encapsulated graphene samples. Nevertheless, the results of TPS measurements showed that rectified and sharp photocurrents can be achieved as a consequence of the complete passivation of graphene with the PED grown SiO_2 layer. The experimentally obtained results can be used as a pioneering model for improving long-term electrical and optoelectronic stability of graphene-based devices.

ACKNOWLEDGMENTS

The authors thank Hasan Aydın for his help on photocurrent spectroscopy measurements and Serap Yiğen for Pulsed Electron Deposition experiments. SEM analyses of the samples were done in the Center for Materials Research of Izmir Institute of Technology.

[1]I. Meric, M. Y. Han, A. F. Young, B. Ozyilmaz, P. Kim, and K. L. Shepard, Nat. Nanotechnol. **3**, 654 (2008).
[2]Y. An, A. Behnam, E. Pop, and A. Ural, Appl. Phys. Lett. **102**, 013110 (2013).
[3]X. Li *et al.*, Small **12**, 595 (2016).
[4]H. Aydın, S. Kalkan, C. Varlikli, and C. Çelebi, Nanotechnology **29**, 145502 (2018).
[5]F. Schedin, A. Geim, S. Morozov, E. Hill, P. Blake, M. Katsnelson, and K. Novoselov, Nat. Mater. **6**, 652 (2007).
[6]S. B. Kalkan, S. Yiğen, and C. Çelebi, Sens. Actuators A **280**, 8 (2018).
[7]S. Rumyantsev, G. Liu, W. Stillman, M. Shur, and A. Balandin, J. Phys. Condens. Matter **22**, 395302 (2010).
[8]A. Sundararajan, M. J. Boland, D. Patrick Hunley, and D. R. Strachan, Appl. Phys. Lett. **103**, 253505 (2013).
[9]G. Skoblin, J. Sun, and A. Yurgens, Appl. Phys. Lett. **110**, 053504 (2017).
[10]T.-J. Ha, D. Akinwande, and A. Dodabalapur, Appl. Phys. Lett. **101**, 033309 (2012).
[11]W. C. Shin, S. Seo, and B. J. Cho, Appl. Phys. Lett. **98**, 153505 (2011).
[12]A. S. Mayorov *et al.*, Nano Lett. **11**, 2396 (2011).
[13]K. Alexandrou, N. Petrone, J. Hone, and I. Kymissis, Appl. Phys. Lett. **106**, 113104 (2015).
[14]P.-H. Ho, Y.-C. Yeh, D.-Y. Wang, S.-S. Li, H.-A. Chen, Y.-H. Chung, C.-C. Lin, W.-H. Wang, and C.-W. Chen, ACS Nano **6**, 6215 (2012).
[15]A. A. Sagade, D. Neumaier, D. Shall, M. Otto, A. Pesquera, A. Centeno, A. Zurutuza, and H. Kurz, Nanoscale **7**, 3558 (2015).
[16]J. A. Alexander-Webber *et al.*, 2D Mater. **4**, 011008 (2017).
[17]Z. A. Van Veldhoven, J. A. Alexander-Webber, A. A. Sagade, P. Braeuninger-Weimer, and S. Hofmann, Phys. Status Solidi B **253**, 2321 (2016).
[18]L. Zheng, X. Cheng, D. Cao, Z. Wang, D. Xu, C. Xia, L. Shen, and Y. Yu, J. Vac. Sci. Technol. A **32**, 01A103 (2014).
[19]Y. J. Kim, Y. G. Lee, U. Jung, S. Lee, S. K. Lee, and B. H. Lee, Nanoscale **7**, 4013 (2015).
[20]D. A. Deen, J. G. Champlain, and S. J. Koester, Appl. Phys. Lett. **103**, 073504 (2013).
[21]S. Kalkan, H. Aydın, D. Özkendir, and C. Çelebi, Appl. Phys. Lett. **112**, 013103 (2018).
[22]M. Song *et al.*, Sci. Adv. **3**, e1602188 (2017).
[23]Q. Jiang, Z. Ao, and Q. Jiang, Phys. Chem. Chem. Phys. **15**, 10859 (2013).
[24]Z. Xu, Z. Ao, D. Chu, A. Younis, C. M. Li, and S. Li, Sci. Rep. **4**, 6450 (2014).
[25]K. Brenner, Y. Yang, and R. Murali, Carbon **50**, 637 (2012).
[26]R. Jaaniso *et al.*, Sens. Actuators B Chem. **190**, 1006 (2014).
[27]A. Dey, A. Chroneos, N. S. J. Braithwaite, R. P. Gandhiraman, and S. Krishnamurthy, Appl. Phys. Rev. **3**, 021301 (2016).
[28]Y. J. Shin, Y. Wang, H. Huang, G. Kalon, A. T. S. Wee, Z. Shen, C. S. Bhatia, and H. Yang, Langmuir **26**, 3798 (2010).
[29]J. Robertson, Mater. Sci. Eng. R **37**, 129 (2002).
[30]F. Walther, P. Davydovskaya, S. Zürcher, M. Kaiser, H. Herberg, A. M. Gigler, and R. W. Stark, J. Micromech. Microeng. **17**, 524 (2007).
[31]N.-K. Park, Y. S. Kim, M. J. Kim, T. J. Lee, S. H. Lee, and S. H. Lee, J. Nanosci. Nanotechnol. **13**, 7493 (2013).
[32]U. Schulz, S. Jakobs, and N. Kaiser, Proc. SPIE **2776**, 169 (1996).
[33]L. Van der Pauw, Philips Res. Rep. **13**, 1 (1958).
[34]F. Werner, J. Appl. Phys. **122**, 135306 (2017).
[35]J. Park, A. Reina, R. Saito, J. Kong, G. Dresselhaus, and M. Dresselhaus, Carbon **47**, 1303 (2009).
[36]A. Reina, X. Jia, J. Ho, D. Nezich, H. Son, V. Bulovic, M. S. Dresselhaus, and J. Kong, Nano Lett. **9**, 30 (2008).
[37]Z. Lin, X. Ye, J. Han, Q. Chen, P. Fan, H. Zhang, D. Xie, H. Zhu, and M. Zhong, Sci. Rep. **5**, 11662 (2015).
[38]H. Tada, A. E. Kumpel, R. E. Lathrop, J. B. Slanina, P. Nieva, P. Zavracky, I. N. Miaoulis, and P. Y. Wong, J. Appl. Phys. **87**, 4189 (2000).
[39]D. Yoon, Y.-W. Son, and H. Cheong, Nano Lett. **11**, 3227 (2011).
[40]M. Aliofkhazraei, *Wetting and Wettability* (InTech, London, 2015).
[41]X. Liang, Z. Fu, and S. Y. Chou, Nano Lett. **7**, 3840 (2007).
[42]C. G. Kang, Y. G. Lee, S. K. Lee, E. Park, C. Cho, S. K. Lim, H. J. Hwang, and B. H. Lee, Carbon **53**, 182 (2013).
[43]J. Robertson, Eur. Phys. J. Appl. Phys. **28**, 265 (2004).
[44]J. Kolodzey, E. A. Chowdhury, T. N. Adam, G. Qui, I. Rau, J. O. Olowolafe, J. S. Suehle, and Y. Chen, IEEE Trans. Electron Devices **47**, 121 (2000).
[45]Y. Yang and R. Murali, Appl. Phys. Lett. **98**, 093116 (2011).
[46]J. W. Suk, W. H. Lee, J. Lee, H. Chou, R. D. Piner, Y. Hao, D. Akinwande, and R. S. Ruoff, Nano Lett. **13**, 1462 (2013).
[47]A. Pirkle *et al.*, Appl. Phys. Lett. **99**, 122108 (2011).
[48]S. Ryu, L. Liu, S. Berciaud, Y.-J. Yu, H. Liu, P. Kim, G. W. Flynn, and L. E. Brus, Nano Lett. **10**, 4944 (2010).
[49]J. Estrada and J. Duszczyk, J. Mater. Sci. **26**, 3909 (1991).